# High-Throughput Bubble Screening Method for Combinatorial Discovery of Electrocatalysts for Water Splitting

Chengxiang Xiang,*[,†] Santosh K. Suram,[†] Joel A. Haber,[†] Dan W. Guevarra,[†] Ed Soedarmadji,[†] Jian Jin,[‡] and John M. Gregoire*[,†]

[†]Joint Center for Artificial Photosynthesis, California Institute of Technology, Pasadena California 91125, United States

[‡]Engineering Division and Joint Center for Artificial Photosynthesis, Lawrence Berkeley National Laboratory, Berkeley California 94720, United States

Ⓢ *Supporting Information*

**ABSTRACT:** Combinatorial synthesis and screening for discovery of electrocatalysts has received increasing attention, particularly for energy-related technologies. High-throughput discovery strategies typically employ a fast, reliable initial screening technique that is able to identify active catalyst composition regions. Traditional electrochemical characterization via current−voltage measurements is inherently throughput-limited, as such measurements are most readily performed by serial screening. Parallel screening methods can yield much higher throughput and generally require the use of an indirect measurement of catalytic activity. In a water-splitting reaction, the change of local pH or the presence of oxygen and hydrogen in the solution can be utilized for parallel screening of active electrocatalysts. Previously reported techniques for measuring these signals typically function in a narrow pH range and are not suitable for both strong acidic and basic environments. A simple approach to screen the electrocatalytic activities by imaging the oxygen and hydrogen bubbles produced by the oxygen evolution reaction (OER) and hydrogen evolution reaction (HER) is reported here. A custom built electrochemical cell was employed to record the bubble evolution during the screening, where the testing materials were subject to desired electrochemical potentials. The transient of the bubble intensity obtained from the screening was quantitatively analyzed to yield a bubble figure of merit (FOM) that represents the reaction rate. Active catalysts in a pseudoternary material library, (Ni−Fe−Co)O$_x$, which contains 231 unique compositions, were identified in less than one minute using the bubble screening method. An independent, serial screening method on the same material library exhibited excellent agreement with the parallel bubble screening. This general approach is highly parallel and is independent of solution pH.

**KEYWORDS:** high-throughput screening, electrocatalyst, water-splitting, oxygen evolution reaction, inkjet printing
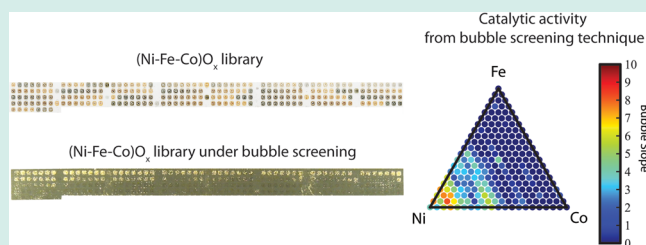
Discovery of electrocatalysts for water splitting reactions, the oxygen evolution reaction (OER) and the hydrogen evolution reaction (HER), has received increasing attention. These electrocatalysts are critical components in a solar-to-hydrogen generator or in an electrolyzer. Large-scale implementation of devices performing the water-splitting reaction requires a highly conductive media and product separation using a proton or hydroxide exchange membrane.[1,2] Thus, electrocatalysts that are stable and can efficiently operate in strong base and strong acid are exceedingly important. The state-of-the-art electrocatalysts for HER and OER in acid contain noble metals and metal oxides, such as Pt and RuO$_2$, which operate at 55 mV and 270 mV overpotential at 10 mA cm$^{-2}$ for HER and OER, respectively.[3,4] Discovery of cheap, earth abundant electrocatalysts to replace these noble metals and metal oxides has been a major effort in the community. Some of the best electrocatalyst reported to date operate in alkaline media and include Ni−Mo alloys for the HER (overpotential of 75 mV at 10 mA cm$^{-2}$ with a Tafel slope of 40 mV/dec) and (Fe−Ni)O$_x$ alloys for the OER

(overpotential of 280 mV at 10 mA cm$^{-2}$ with a Tafel slope of 40 mV/dec).[5,6] Higher-order composition spaces containing three or more metals offer promise of improved electrocatalytic performance, but synthesis and characterization of these material compositions remains a formidable task, simply because the number of the compositions is very large (with 5% composition steps, 231 for a ternary, 1771 for a quaternary, and 10 626 for a quinary libraries).

High-throughput materials synthesis and screening can play a significant role in material discoveries of electrocatalysts. Combinatorial techniques have only recently been employed for the discovery of photocatalysts and materials for photo-electrochemical applications, yielding several reports on the screening of composition libraries. Imaging pH[7,8] or color resulting from changes of florescence signals[9,10] or organic

dyes[11−14] were reported as highly parallel screening methods for photocatalysts. These two-dimensional indicators of catalysis were typically functional in a narrow pH range and in particular were not suitable for either strongly acidic or basic environments. Moreover, most florescence quenching molecules or organic dyes are not sensitive to the presence of hydrogen, which makes the screening for HER electrocatalysts exceedingly difficult.

In this work, we describe a simple approach for screening electrocatalytic activity by imaging the bubble evolution resulting from electrocatalysis of the HER and OER. This general approach is highly parallel and can be adapted to all pH ranges. Using the bubble screening technique, we mapped the electrocatalytic activity of the OER for a pseudoternary material library, $(Ni-Fe-Co)O_x$, with a 5% composition step. After application of an electrochemical potential between the sample materials and a custom-built counter electrode for less than one minute, the images of bubble evolution were analyzed to identify composition regions with high catalytic activities.

The fidelity of the parallel screening method was demonstrated using OER catalysts with known relative activity. Randomly distributed $FeNiO_x$, $FeO_x$, and $TiO_x$ samples were prepared on an FTO coated glass by inkjet printing, where the prepared $FeNiO_x$ is known to be a significantly better OER catalyst than the other two materials.[16] Figure 1a shows the
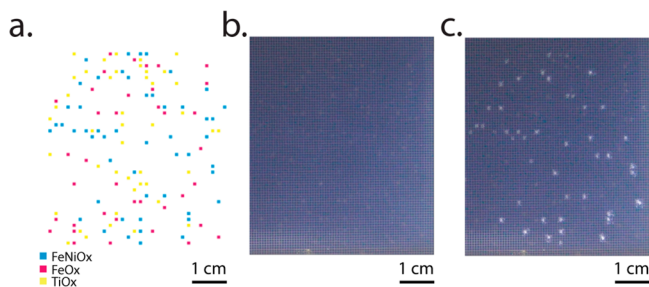


**Figure 1.** Proof-of-concept bubble evolution results from three different electrocatalysts randomly populated on an FTO coated glass. (a) The sample distributions of three electrocatalyst compositions are shown as cyan ($FeNiO_x$), magenta ($FeO_x$), and yellow ($TiO_x$). (b) A snapshot of the bubble evolution video at $t = 0$. c). A snapshot of the bubble evolution video at $t = 25$ s showing registration with the $FeNiO_x$ catalysts.

printed library for the three electrocatalysts on the FTO coated glass. The sample spot size is 1 mm × 1 mm and the minimal center-to-center spacing between two sample spots is 2 mm. Figure 1b and 1c show snap-shots of the bubble evolution at $t = 0$ s and $t = 25$ s, respectively. After applying the electrochemical potential (750 mV vs Ag/AgCl, approximately 500 mV OER overpotential) for a few seconds, the $FeNiO_x$ samples showed strong bubble signals. The observed bubble signals came from both the oxygen bubbles that were nucleated at the testing plate and in the electrolyte and the hydrogen bubbles that were produced at the counter mesh electrode. Because of the small distance between the working electrode and the counter electrode, excellent spatial registration was observed between sample spots and bubble signals. From the bubble intensity, the $FeNiO_x$ samples are readily identified as the most active catalysts on the testing plate.

To demonstrate the utility of the high-throughput bubble screening method in catalyst discovery, the technique was applied to a $(Ni-Fe-Co)O_x$ pseudoternary material library.

Camera images of the samples acquired before applying the electrochemical potential, after applying the electrochemical potential (750 mV vs Ag/AgCl, approximately 500 mV OER overpotential) at $t = 0$ s, and during the bubble experiment at $t = 20$ s are shown in Figure 2b, 2c and 2d, respectively. Figure
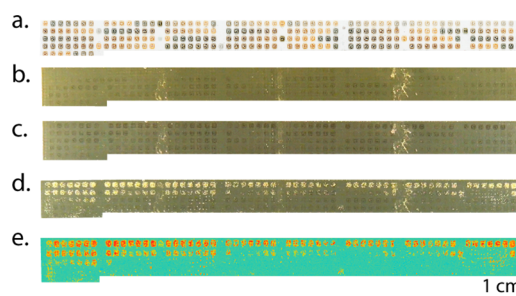


**Figure 2.** (a) Optical images of a pseudoternary material library, $(Ni-Fe-Co)O_x$. (b) Snap-shots of the bubble evolution before applying the electrochemical potential and after application of the electrochemical potential (750 mV vs Ag/AgCl) at 0 s (c) and 20 s (d). (e). Background subtracted bubble image at 20 s. Note that the bright pixels in panel b are an artifact from the substrate (not bubbles) and are effectively removed by the background subtraction, as shown in panel e.

2e shows a background-subtracted bubble image at $t = 20$ s. Comparing Figure 2b and Figure 2c, a significant color change due to the redox reactions in the Ni-containing films was observed before and after applying the electrochemical potential.

Figure 3 shows the bubble intensity as a function of time for three representative samples in the material library. The most
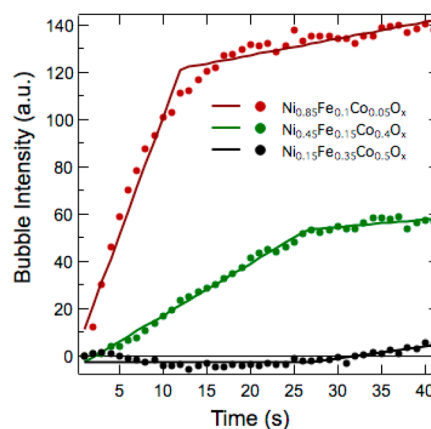


**Figure 3.** Bubble intensity as a function of time for an active catalyst (red), a moderate catalyst (green) and an inactive catalyst (black), where the solid lines were fitted data with two distinctive slopes.

active catalyst (red, $Ni_{0.85}Fe_{0.1}Co_{0.05}O_x$) exhibited a fast increase in the bubble intensity for the first 15 s and gradually reached a quasi-steady state bubble intensity. The moderate catalyst (green, $Ni_{0.45}Fe_{0.15}Co_{0.4}O_x$) showed a slower increase in the bubble intensity and reached a lower quasi-steady state bubble intensity. The relatively inactive catalyst (black, $Ni_{0.15}Fe_{0.35}Co_{0.5}$) showed minimal change in the bubble intensity. The time transient of bubble data was then fit with two linear regions with the slope of the first segment being significantly larger than that of the second linear segment for the vast majority of samples. Some noisy bubble intensity
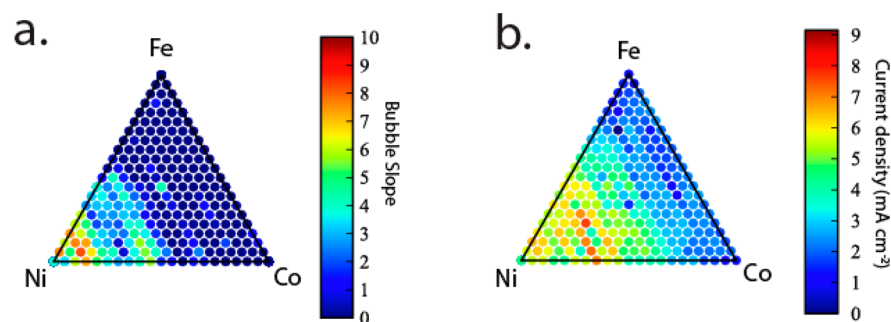
**Figure 4.** (Ni−Fe−Co)O$_x$ pseudoternary compositional maps of catalyst Figures of merit: (a) The bubble evolution slope from the parallel bubble screening and (b) the current density at 750 mv vs Ag/AgCl from serial scanning droplet cell measurement.
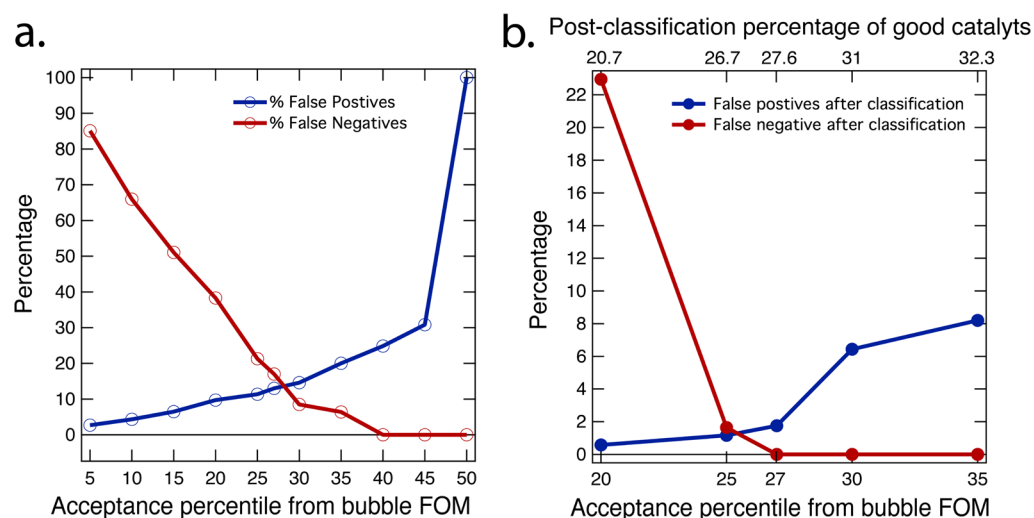


**Figure 5.** False positive percentage and false negative percentage as a function of the acceptance percentile from the bubble FOM before (Figure 5a) and after (Figure 5b) a support-vector machine (SVM) based classification method was applied to the bubble data and the SDC data independently. Catalysts from the top 20 percentile of the SDC FOM (see Figure 4b) were defined as "good" catalysts. In Figure 5b, the top axis provides the percentage of good catalysts identified by applying the classification method to the set of samples given by the acceptance percentile on the bottom axis.

signals did not exhibit the model sequence of two linear regions and thus the larger slope from the fitting routine was assigned as the figure of merit (FOM).

It is worth noting that for the geometry of our library and test cell, we observe significant artifacts for experiments lasting longer than 40 s. Local convection currents in the solution cause spreading of the generated bubbles such that after 40 s the lateral motion of bubbles begins to exceed 1 mm, causing loss of sample-specific spatial resolution. We also observe that on this time scale, O$_2$ bubbles generated at the working electrode release from the surface and accumulate at the counter electrode, allowing for the oxygen reduction reaction to compete with the hydrogen evolution reaction at the counter electrode. The deleterious effects of this bubble crossover include a decline in bubble production rate.

Figure 4a shows the calculated FOM from the bubble screening for the quasi-ternary material library, where the most active catalysts were identified at Ni-rich compositions. To validate the parallel bubble screening results, we carried out serial measurements of the electrocatalytic performance of the same library using a scanning droplet cell (SDC).[16] The detailed cell design and operation were described by Gregoire et al.[16] Briefly, a solution droplet was employed to make contact to the sample of interest. A Ag/AgCl reference electrode and a Pt counter electrode were electrically

incorporated into the droplet cell to ensure minimal uncompensated resistive loss. A 20 s chronoamperometry measurement was performed for each sample using the same potential as the bubble experiment, 750 mV vs Ag/AgCl. The FOM was calculated as the average catalytic current density over the last 2 s of the measurement, and the composition map is plotted in Figure 4b. From Figure 4a and 4b, a similar trend for catalyst activity was observed in the compositional space from two independent screening techniques.

To further quantitatively understand the correlation between two screening techniques, the SDC data of Figure 4b was taken to be the control data and the top 20 percentile of the compositions were taken as the control set of "good" catalysts. For an unexplored composition space, the fraction of high performance catalysts will generally be much lower, but a composition library with known catalysts was selected for the demonstration of the bubble screening technique. The ability of the bubble screening technique to reproduce this set of good catalysts was quantified by calculating false negative and false positive percentages assuming that top $x$ percentile of bubble data can be considered as good catalysts; wherein $x$ was varied from 5 to 50. Catalysts that are represented as good catalysts in the bubble screening and are not represented as good catalysts in SDC data are false positives. Whereas catalysts that are not represented as good catalysts in bubble data but are represented
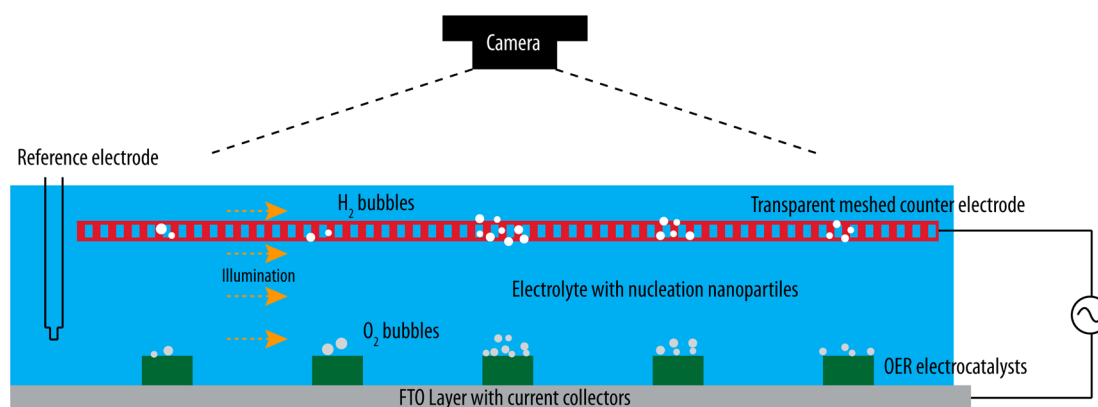
**Figure 6.** Cross-sectional schematic illustration of the bubble screening setup, where the green rectangles represent the testing material library, the red bars represent the transparent meshed counter electrode.

as good catalysts in the SDC data are false negatives. False positive and false negative percentages are defined as

$$\% \text{ false positives} = \frac{\text{no. of false positives}}{\text{no. of SDC bad catalysts}} \times 100 \quad (1)$$

$$\% \text{ false negatives} = \frac{\text{no. of false negatives}}{\text{no. of SDC good catalysts}} \times 100 \quad (2)$$

False positives increase the work load for subsequent experiments, while false negatives are more undesirable as they may lead to failed detection of active catalysts. Figure 5a shows the false positive and false negative percentages for several acceptance percentiles of the bubble FOM. Figure 5a shows that an acceptance rate near 30 percentile of catalysts in bubble screening is near-optimal for the dual objective of minimizing false negatives and false positives. Using this acceptance for bubble screening captures top 20 percentile of active catalysts in SDC measurements with a false negative percentage of 8.5% and a false positive percentage of 14.6%.

To further improve the statistical correlation between the two measurements, we applied a support-vector machine (SVM) based classification method[19,20] in the composition space. In both screening techniques, local composition regions of good catalysts occasionally contain an outlier bad catalyst, which is problematic for the sample-by-sample comparison. The objective of utilizing SVM classification is to identify composition regions of good and bad catalysts in SDC and bubble data independently. By comparison of these post-classified data sets, we can evaluate the ability of the bubble screening technique to identify composition regions containing active catalysts. Several SVM classifiers were independently trained assuming top 20 percentile catalysts were good in the SDC data and top $x$ percentile catalysts were good in the bubble data; wherein $x = 20, 25, 27, 30, 35$ (Figure 5b). In each instance, the classification algorithm takes the training data and assigns appropriate weights to samples in neighborhood compositions to identify composition regions of good and bad catalysts. The false positive percentage and the false negative percentage of the FOM after classification (Figure 5b) are much lower due to the removal of low-FOM outliers. For example, using a preclassification acceptance rate of top 27 percentile for the bubble data and top 20 percentile for the SDC data, we obtain a false negative percentage of 0% and a false positive percentage of 1.75%. The identified good catalysts

before and after classification using the percentiles described above in both screening methods are illustrated in the Supporting Information (Figure S2). In this example, it is useful to note that while a preclassification acceptance rate of top 20 percentile was chosen for the SDC data, the outlier rejection of the classification technique expanded the set of good catalysts to 26.3% of the samples. Similarly, with an acceptance rate of top 27 percentile for the bubble data, postclassification results identify 27.6% as good according to the bubble screen technique. These results show that the parallel bubble screening method rapidly identifies active catalysts, and that with the additional application of the classification method, the composition regions of best performing catalysts are identified with no false negatives and a low false positive rate.

In this work, we have demonstrated an efficient and highly parallel bubble-screening method for combinatorial discovery of OER catalysts. We screened a $(Ni-Fe-Co)O_x$ pseudoternary electrocatalyst library using this method and identified the most active electrocatalysts in less than one minute. An independent serial screening on the same material library using a scanning droplet cell (SDC) was employed to validate the bubble screening. After application of a support-vector machine (SVM) based classification method, 0% false negative and 1.75% false positive rates were obtained between the top 20 percentile of the SDC measurements and the top 27 percentile of the bubble screening data. The reported technique is pH independent and can also be employed for screening HER catalysts.

■ **EXPERIMENTAL PROCEDURES**

**Bubble Screening Setup.** The cross-sectional detailed experimental setup for the bubble screening is illustrated in Figure 6. The working electrode was comprised of an array of catalysts (green rectangles) supported on $SnO_2$:F (FTO)-coated glass. Two line current collectors (adhesive copper tape) were attached along the edges of the material library to provide ample ohmic contact to each catalyst sample through the conducting FTO coating. A highly transparent and conductive Ni mesh (30 Ni mesh, Precision Electroforming LLC) was attached evenly to an acrylic glass and was employed as the counter electrode (red bars). The distance between the working electrode and the counter electrode was controlled by a Teflon spacer with a height of approximately 2 mm. A Ag/AgCl reference electrode was placed 5 mm away from the working electrode-counter electrode assembly. $TiO_2$ nano-

particles (Sigma Aldrich, 21 nm particle size, 62.6 $\mu$M) were suspended in the testing solution using an ultrasonic bath for 10 min and served as bubble nucleation agents for dissolved $O_2$ and $H_2$ gases evolved at the working and counter electrodes, respectively. During the screening, a source meter (Keithley 2400) was used to apply a voltage bias between the working electrode and the counter electrode, while a Multimeter (Keithley 2000) was used to measure the electrochemical potential between the working electrode and the reference electrode. Alternatively, a Gamry potentiostat was used to apply electrochemical potentials as a traditional three-electrode setup. A strip of LEDs was employed for side-illumination during screening to enhance the bubble contrast. A commercial camcorder (SONY, HDR-CX380) was mounted above the working electrode-counter electrode assembly to capture the evolution of the bubbles during the screening. Before the bubble screening, a white Teflon sheet was inserted underneath the working electrode-counter electrode assembly to ease identification of the sample material spots in the camera image. Before commencing the electrochemical experiment, the white Teflon sheet was replaced with a black sheet to enhance the contrast of the gas bubbles in the camcorder images. Images of bubble formation and growth were acquired at the native camcorder acquisition rate of 48 frames/s during the electrochemical experiment.

**Material Library Synthesis.** The discrete pseudoternary $(Ni-Fe-Co)O_x$ library with 5.0 at % composition steps for each of Ni, Fe and Co was designed as a grid of individual samples. The complete array of 231 samples was deposited by inkjet printing onto the FTO-coated side of a 10 cm ×15 cm glass plate at a resolution of 2880 × 1440 dpi, as described previously.[15,16] Four separate metal inks, of the type previously described by Fan and Stuckey,[17,18] were prepared by mixing 5 mmol of each of the Ni, Fe, and Co precursor with 0.80 g Pluronic F127 (Aldrich), 1.0 mL glacial acetic acid (T.J. Baker, Inc.), 0.40 mL of concentrated $HNO_3$ (EMD), and 30 mL of 200 proof Ethanol (Koptec). The metal precursors were $Ni(NO_3)_2 \cdot 6H_2O$ (1.53 g, 99.999%, Sigma Aldrich), $Fe(NO_3)_3 \cdot 9H_2O$ (2.14 g, ≥98%, Sigma Aldrich) and $Co(NO_3)_2 \cdot 6H_2O$ (1.46 g, 99.99%, Sigma Aldrich). After the library of compositions was printed as a set of 1 mm × 1 mm spots on a 2 mm pitch, the inks were dried and the metal precursors converted to metal oxides by calcination in air at 40 °C for 18 h, then at 70 °C for 24 h, followed by a 5 h ramp and 10 h soak at 350 °C.

**Data Analysis.** Upon application of the anodic electrochemical potential, many samples undergo an oxidation reaction that causes a rapid change in the sample color. The visual appearance of the catalysts stabilizes after approximately 2 s, at which time no bubbles have yet formed, and this time is chosen as the $t = 0$ commencement of the bubble experiment. The video data starting at this time is analyzed using custom routines to extract the bubble evolution for each sample. The raw video file was first converted into a greyscale image sequence and the background image acquired at $t = 0$ was subtracted from all subsequent images. For each sample the corresponding region of 140 pixels was parsed from each image and the bubble intensity was calculated as the sum of the pixels' greyscale intensities.

During the course of the bubble screening (typically 20−40 s), most active samples showed an immediate linear increase in the bubble intensity which transitioned to a slower, quasi-steady state increase in bubble intensity related to several saturation phenomena. Since different samples reach this transition point at different times, the selection of the bubble intensity at an arbitrarily chosen time can introduce significant artifacts into the relative bubble intensity. A more robust figure of merit (FOM) was calculated as the slope of the initial linear increase in bubble intensity, which was extracted from a custom regression fitting routine. In addition to the linear fit parameters, the least-squares regression routine included the transition time as a fit parameter.

## ■ ASSOCIATED CONTENT

**Ⓢ Supporting Information**
Additional information about support vector machines and application and figures showing a false color representation of the the mean three-fold validation scores and ternary compositional maps. This material is available free of charge via the Internet at http://pubs.acs.org.

## ■ AUTHOR INFORMATION

**Corresponding Authors**
*E-mail: cxx@caltech.edu.
*E-mail: gregoire@caltech.edu.

**Notes**
The authors declare no competing financial interest.

## ■ REFERENCES

(1) Haussener, S.; Xiang, C. X.; Spurgeon, J. M.; Ardo, S.; Lewis, N. S.; Weber, A. Z. Modeling, simulation, and design criteria for photoelectrochemical water-splitting systems. *Energy Environ. Sci.* **2012**, *5* (12), 9922−9935.

(2) Lewis, N. S. Systematic development of an artificial solar-fuel generation device. *Abstr. Papers Am. Chem. Soc.* **2013**, 245.

(3) Trasatti, S. Work function, electronegativity, and electrochemical behavior of metals 0.3. Electrolytic hydrogen evolution in acid solutions. *J. Electroanal. Chem.* **1972**, *39* (1), 163.

(4) McCrory, C. C. L.; Jung, S.; Peters, J. C.; Jaramillo, T. F. Benchmarking heterogeneous electrocatalysts for the oxygen evolution reaction. *J. Am. Chem. Soc.* **2013**, *135* (45), 16977−16987.

(5) Brown, D. E.; Mahmood, M. N.; Turner, A. K.; Hall, S. M.; Fogarty, P. O. Low overvoltage electrocatalysts for hydrogen evolving electrodes. *Int. J. Hydrogen Energy* **1982**, *7* (5), 405−410.

(6) Landon, J.; Demeter, E.; Inoglu, N.; Keturakis, C.; Wachs, I. E.; Vasic, R.; Frenkel, A. I.; Kitchin, J. R. Spectroscopic characterization of mixed Fe−Ni oxide electrocatalysts for the oxygen evolution reaction in alkaline electrolytes. *ACS Catal.* **2012**, *2* (8), 1793−1801.

(7) Matsumoto, Y.; Murakami, M.; Jin, Z. W.; Nakayama, A.; Yamaguchi, T.; Ohmori, T.; Suzuki, E.; Nomura, S.; Kawasaki, M.; Koinuma, H. Combinatorial synthesis and high throughput evaluation of doped $TiO_2$ thin films for the development of photocatalysts. *Comb. Compos. Spread Tech. Mater. Device Dev.* **2000**, *3941*, 19−27.

(8) Nakayama, A.; Suzuki, E.; Ohmori, T. Development of high throughput evaluation for photocatalyst thin-film. *Appl. Surf. Sci.* **2002**, *189* (3−4), 260−264.

(9) Gerken, J. B.; Chen, J. Y. C.; Masse, R. C.; Powell, A. B.; Stahl, S. S. Development of an O-2-sensitive fluorescence-quenching assay for the combinatorial discovery of electrocatalysts for water oxidation. *Angew. Chem., Int. Ed.* **2012**, *51* (27), 6676−6680.

(10) Dai, Q. X.; Xiao, H. Y.; Li, W. S.; Na, Y. Q.; Zhou, X. P. Photodegradation catalyst discovery by high-throughput experiment. *J. Comb. Chem.* **2005**, *7* (4), 539−545.

(11) Kafizas, A.; Adriaens, D.; Mills, A.; Parkin, I. P. Simple method for the rapid simultaneous screening of photocatalytic activity over multiple positions of self-cleaning films. *Phys. Chem. Chem. Phys.* **2009**, *11* (37), 8367−8375.

(12) Ding, J. J.; Bao, J.; Sun, S. N.; Luo, Z. L.; Gao, C. Combinatorial discovery of visible-light driven photocatalysts based on the ABO(3)-type (A = Y, La, Nd, Sm, Eu, Gd, Dy, Yb, B = Al and In) binary oxides. *J. Comb. Chem.* **2009**, *11* (4), 523−526.

(13) Kafizas, A.; Parkin, I. P. The combinatorial atmospheric pressure chemical vapour deposition (cAPCVD) of a gradating N-doped mixed phase titania thin film. *J. Mater. Chem.* **2010**, *20* (11), 2157−2169.

(14) Kafizas, A.; Mills, A.; Parkin, I. P. A comprehensive aerosol spray method for the rapid photocatalytic grid area analysis of semiconductor photocatalyst thin films. *Anal. Chim. Acta* **2010**, *663* (1), 69−76.

(15) Gregoire, J. M.; Xiang, C.; Mitrovic, S.; Liu, X.; Marcin, M.; Cornell, E. W.; Fan, J.; Jin, J. Combined catalysis and optical screening for high throuphut discovery of solar fuels catalysts. *J. Electrochem. Soc.* **2013**, *160* (4), F337−F342.

(16) Gregoire, J. M.; Xiang, C. X.; Liu, X. N.; Marcin, M.; Jin, J. Scanning droplet cell for high throuphut electrochemical and photoelectrochemical measurements. *Rev. Sci. Instrum.* **2013**, *84*, 2.

(17) Fan, J.; Boettcher, S. W.; Stucky, G. D. Nanoparticle assembly of ordered multicomponent mesostructured metal oxides via a versatile sol−gel process. *Chem. Mater.* **2006**, *18* (26), 6391−6396.

(18) Liu, X. N.; Shen, Y.; Yang, R. T.; Zou, S. H.; Ji, X. L.; Shi, L.; Zhang, Y. C.; Liu, D. Y.; Xiao, L. P.; Zheng, X. M.; Li, S.; Fan, J.; Stucky, G. D. Inkjet printing assisted synthesis of multicomponent mesoporous metal oxides for ultrafast catalyst exploration. *Nano Lett.* **2012**, *12* (11), 5733−5739.

(19) Cortes, C.; Vapnik, V. Support-vector networks. *Mach. Learn.* **1995**, *20* (3), 273−297.

(20) Press, W. H.; Teukolsky, S. A.; Vetterling, W. T.; Flannery, B. P. *Numerical Recipes: The Art of Scientific Computing*, 3rd ed.; Cambridge University Press: Cambridge, U.K., 2007.